

# Achieving 100X faster simulations of complex biological phenomena by coupling ML to HPC ensembles

Alexander Brace

abrace@anl.gov  
Data Science & Learning Division,  
Argonne National Laboratory

Anda Trifan

atrifan2@illinois.edu  
University of Illinois at  
Urbana-Champaign  
Data Science & Learning Division,  
Argonne National Laboratory

Todd Munson

tmunson@mcs.anl.gov  
Mathematics & Computer Science  
Division, Argonne National  
Laboratory

Hyungro Lee

hyungro.lee@rutgers.edu  
RADICAL, ECE, Rutgers University

Matteo Turilli

matteo.turilli@rutgers.edu  
RADICAL, ECE, Rutgers University

Ian Foster

foster@uchicago.edu  
Data Science & Learning Division,  
Argonne National Laboratory  
University of Chicago

Arvind Ramanathan

ramanathana@anl.gov  
Data Science & Learning Division,  
Argonne National Laboratory  
University of Chicago

Heng Ma

heng.ma@anl.gov  
Data Science & Learning Division,  
Argonne National Laboratory

Igor Yakushin

iyakushin@anl.gov  
Data Science & Learning Division,  
Argonne National Laboratory

Shantenu Jha

shantenu@bnl.gov  
Brookhaven National Laboratory  
RADICAL, ECE, Rutgers University

## ABSTRACT

The use of ML methods to dynamically steer ensemble-based simulations promises significant improvements in the performance of scientific applications. We present DeepDriveMD, a tool for a range of prototypical ML-driven HPC simulation scenarios, and use it to quantify improvements in the scientific performance of ML-driven ensemble-based applications. We discuss its design and characterize its performance. Motivated by the potential for further scientific improvements and applicability to more sophisticated physical systems, we extend the design of DeepDriveMD to support stream-based communication between simulations and learning methods. It demonstrates a 100x speedup to fold proteins, and performs 1.6x more simulations per unit time, improving resource utilization compared to the sequential framework. Experiments are performed on leadership-class platforms, at scales of up to O(1000) nodes, and for production workloads. We establish DeepDriveMD as a high-performance framework for ML-driven HPC simulation scenarios, that supports diverse simulation and ML back-ends, and

which enables new scientific insights by improving length- and time-scale accessed.

## KEYWORDS

multi-scale molecular simulations, machine learning, workflow, complex biological systems

## ACM Reference Format:

Alexander Brace, Hyungro Lee, Heng Ma, Anda Trifan, Matteo Turilli, Igor Yakushin, Todd Munson, Ian Foster, Shantenu Jha, and Arvind Ramanathan. 2018. Achieving 100X faster simulations of complex biological phenomena by coupling ML to HPC ensembles. In *SC'21: The International Conference for High Performance Computing, Networking, Storage, and Analysis, November 14–19, 2021, St Louis, MO*. ACM, New York, NY, USA, 13 pages. <https://doi.org/10.1145/1122445.1122456>

## 1 INTRODUCTION

Scientific high-performance computing (HPC) has traditionally focused on enhancing the scale and performance of a single large task. However, the end of Dennard scaling and the realities of post-Moore parallelism place increasingly severe limitations on the ability of single monolithic applications to achieve significant performance gains on large-scale parallel machines. A fundamental re-examination of computational methods and application architectures and how they overcome performance and heterogeneity barrier of future platforms is required.

Permission to make digital or hard copies of all or part of this work for personal or classroom use is granted without fee provided that copies are not made or distributed for profit or commercial advantage and that copies bear this notice and the full citation on the first page. Copyrights for components of this work owned by others than ACM must be honored. Abstracting with credit is permitted. To copy otherwise, or republish, to post on servers or to redistribute to lists, requires prior specific permission and/or a fee. Request permissions from [permissions@acm.org](mailto:permissions@acm.org).  
*SC'21, November 14–19, 2021, St Louis, MO*

© 2018 Association for Computing Machinery.  
ACM ISBN 978-1-4503-9999-9/18/06...\$15.00  
<https://doi.org/10.1145/1122445.1122456>

In response, HPC scientific applications are seeking new methods for reducing time to scientific insight, such as the use of ensemble simulations [1, 2] and the integration of artificial intelligence (AI) and machine learning (ML) methodologies with traditional HPC applications. AI/ML methods are being used, for example, to steer ensembles of multiscale molecular dynamics (MD) simulations [3, 4] and to dynamically steer or drive simulations to enable efficient exploration of phase space. These and other application scenarios have spurred a growing variety of ML-driven simulation workflows [5, 6], including the use of a single ML model to drive multiple (ensemble) simulations and the use of an ensemble of models, varying, for example, in their parameterization or neural architecture, each steering distinct ensemble simulations concurrently. In these and other scenarios, the ML model may be trained dynamically, or even retrained periodically, typically in a *streaming* or *in situ* manner. ML and simulation phases may be linked either synchronously or asynchronously. In general, ML-driven workflows are characterized by a wide variety of temporal and data coupling between simulations and ML components, introducing a variety of resource and task execution management, scalability, and performance challenges.

We present here **DeepDriveMD**, a high-performance tool designed to support a wide range of ML-driven HPC simulation scenarios and their different types, frequencies, and strengths of coupling of ML methods and HPC simulations. In particular, we examine two design strategies: (1) *sequential implementation* of the DeepDriveMD, called *DeepDriveMD-F*, where the MD simulations are followed by AI/ML training and subsequent inference runs; and (2) *streaming implementation* of DeepDriveMD, referred to as *DeepDriveMD-S*, that enables the independent and concurrent runs of MD and AI/ML tasks, however, with the ability that the individual tasks may exchange data at runtime. In DeepDriveMD-S, the tasks can still be interdependent, based on how simulations are selected using AI/ML methods to run next, since the process remains iterative. We evaluate DeepDriveMD for two different application scenarios, where we demonstrate how ML-driven HPC workflows provide at least an order of magnitude performance improvement over traditional (i.e., non-ML driven) simulation techniques. The scientific performance enhancement is computed by examining equivalence between physical phenomenon investigated for given computational resources [7].

## 2 RELATED WORK

Enhanced sampling methods and, more generally, adaptive sampling techniques utilize an ensemble of molecular dynamics (MD) simulations [8]. As summarized in Fig. 1, these methods include a general computational motif consisting of a parallel set of  $N$  MD simulations, from which different ‘views’ of the data are extracted. Extracting views from the simulation data can involve pre-processing steps that include actions such as filtering only a subset of atoms of interest, or calculating physical parameters (e.g., root-mean squared deviations to a protein’s native state, or radius of gyration, etc.), or simply aggregating conformations from the simulations as they are running. Optionally, various artificial intelligence (AI)/machine learning (ML) techniques can be run across the collective views to guide the next set of simulations to be run.

For example, an AI agent can guide the decisions of which set of simulations must be run next or simply terminating various MD simulations that may not be as productive. More generally, it is also possible to substitute generative models as well as surrogate models that provide access to new conformations from which simulations can be started. This constitutes a *continual learning loop*, providing successive iterations of MD simulations that can be eventually driven automatically, based on AI/ML controls.

While enhanced sampling methods have been widely popular, these methods have only recently been augmented with AI/ML techniques [9, 10, 11, 12, 13]. AI/ML techniques such as reinforcement learning and/or other complementary approaches are discussed elsewhere [14]; however, those earlier reports focused primarily on prototypical systems such as small peptides/proteins to demonstrate this general workflow’s feasibility.

Previous tools for building ML-coupled simulation workflows have focused on integrating popular ML backends, Tensorflow and Pytorch, with simulation toolkits [15, 16, 17]. These frameworks mainly provide a configurable API to specify workflow parameters that optimize the resource utilization of parallel computing resources. Tools such as SmartSim [18] incorporate an HPC job scheduler to orchestrate task assignment and resource allocation through Slurm, Cobalt, or PBSPro. Within multiscale bio-molecular simulations, the recently developed MuMMI [3] framework enables unprecedented sampling capabilities through an iterative combination of multi-scale models, which are “linked” via ML techniques, while simultaneously optimizing HPC resource utilization. Other frameworks, such as NVIDIA SimNet [19] enable AI-driven acceleration of forward and inverse problems in multi-physics (e.g., turbulence), with a particular focus on solving partial differential equations. Much of the recent developments focus on accelerating drug discovery workflows given the immediacy of the ongoing novel coronavirus pandemic (COVID-19) [20, 21, 22, 23].

DeepDriveMD allows users to encapsulate continual learning loops for bio-molecular (and with reasonable extensions to materials science) simulations, and supports a wide range of use cases (see §3). Further, DeepDriveMD can be easily configured to support a variety of AI/ML (including linear, non-linear and hybrid) approaches, AI/ML frameworks (e.g., TensorFlow, PyTorch) as well as simulation backends (e.g., OpenMM, AMBER, NAMD), while allowing for flexible composition between these elements. In this paper, we evaluate the design trade offs, highlighting scientific and computational performance gains when (even simple) ML methods are used to guide the simulation phase space. We hope that such evaluations will provide a baseline for illustrating how HPC workloads coupled to AI/ML approaches accelerate time-to-solution for studying complex/emergent phenomena. Overall, we have built a framework to tightly couple ML to simulation ensembles with flexible configurations and HPC resource management.

## 3 SCIENCE DRIVERS

We outline three representative science drivers that capture the scientific diversity and broad computational requirements. Use case one (UC1) investigates complex/emergent phenomena such as protein folding; UC2 protein-ligand complexes (PLC); and UC3 corresponds to multi-scale modeling, where simulations include the

modeling of an entire virus/viral envelope [24]. UC1 is primarily concerned with studying a single protein system of interest; where as UC2 studies a large number of ligands that interact with and bind to the protein. UC3 includes aspects of scaling simulations to larger systems (i.e.,  $O(100 \times 10^6)$  atoms). UC2 is timely, given the recent COVID-19 pandemic where virtual screening and free energy computations for  $O(10^9)$  ligands has been necessary to identify viable treatments against the virus [22].

**UC1: Protein folding.** Protein folding is a prototypical application for evaluating adaptive sampling techniques. In spite of significant advances in advanced sampling, the state-of-the-art is still several orders of magnitude away what is needed. We posit that machine ML techniques in tandem with simulations, will accelerate the sampling of folding events. To evaluate this postulate, we use a small protein, namely the FSD-EY protein that adopts a  $\beta\beta\alpha$ /BBA fold, consisting of 28 amino-acid residues, to characterize the performance considerations of our ML-integrated workflow. The advantage of using BBA is that it is a relatively fast-folding protein (within  $O(\mu\text{s})$  folding timescales). Further, long timescale simulations of this protein using Anton-1 [25] hardware are readily available to benchmark our ML-integrated workflow against baseline implementations where no ML approaches are used.

**UC2: Protein Ligand Complex.** For studying PLC simulations, our design only considers the aspects of running (and scaling) the number of individual tasks (MD, ML) independently since each ligand is unique and hence there is no need to exchange any information among the tasks explicitly. For this usecase implementation, we consider the novel coronavirus disease/COVID-19 (caused by the severe acute respiratory syndrome coronavirus/SARS-CoV-2) related drug target, papain-like protease (PLPro) against which a number of ligands are evaluated for their binding potency. If a ligand stabilizes the protein when bound, that provides a means to evaluate how it may interact and potentially inhibit PLPro. Although detailed thermodynamic quantities such as free energy of binding are often used to evaluate how ligands interact, to keep our application simpler, we chose to evaluate just the stability of the ligand in PLPro's binding site. In this use case, the number of ligands ( $l$ ) can vary; and simulations per ligand system ( $s$ ) can vary between 1 to  $O(1000)$ , depending on how the simulations are chosen by the ML approach. However, between the runs, there is no information that is exchanged and can be considered essentially as independent DeepDriveMD runs.

**UC3: Multi-scale modeling and simulations of bio-molecular complexes.** The increasing complexity within biological systems has also motivated the development of multiscale simulations, where information from one scale of simulations (e.g., atomistic scale) is transferred to a different scale (e.g., coarse-grained simulation) or between different spatial scales (e.g., individual spike protein vs. spike proteins embedded within a whole virus). These simulations also use ML methods to transfer information across scales; however, given the large number of simulations to be carried out as well as the fact that these bio-molecular systems represent  $O(10^7 - 10^8)$  atoms, we did not explore this workflow in this paper. They do serve as a strong driver for the need for improved scientific and computation efficiency, and thus represent a motivation for DeepDriveMD-S, which we plan to address in future work.

## 4 DESIGN AND IMPLEMENTATION

Coupling ML with HPC simulation ensembles can be visualized as a computational motif highlighted in Fig. 1. In this section, we describe how this general computational motif is realized within DeepDriveMD (§4.1) while also outlining the details of its implementation (§4.3–4.4).

### 4.1 Design

DeepDriveMD supports a class of workflow applications that combine simulation ensembles and ML training computations into a single ML-guided computation. Specifically, DeepDriveMD focuses on workflow applications with five logical components: a *Simulation* component, in which MD simulations are used to explore possible trajectories of a protein (or in general a bio-molecular system of interest); an *Aggregation* component, in which the results of those simulations are combined; an *ML Training* component, in which aggregated trajectories are used to train ML models; a *Selection* component that decides the best model(s) to be used in further iterations or even decide to retrain; and, finally, an *Agent/Surrogate*, in which the trained ML model is used in an 'inference' mode to decide the next set of conformations for further simulations. Since these decisions can be made using AI approaches such as reinforcement learning, we generally refer to this step as an Agent. Furthermore, one may also generalize the instance to include surrogate models, which either accelerate an expensive computational kernel (e.g., modeling electrostatics) or switch between (spatial or temporal) resolution as simulations are running (e.g., learning force field parameters between all-atom and coarse-grained representations).

DeepDriveMD realizes a Python application framework for executing the workflows of the science drivers presented in UC1–UC3 §3 at scale on HPC platforms. Those properties translate to requirements, including: (i) large dynamic range of concurrent simulations that couple to single ML models; (ii) frequency and degree of coupling between simulations and ML models, including switching of HPC and ML tasks; and (iii) coupling a varying number of ML models to ensemble simulations. Put together, these requirements necessitate the design of an extensible software system that supports the generalized coupling of ML with HPC simulations tasks for a range of frequency and volume. For example, in UC1, this may correspond to a measure of sampling effectiveness, which may include how well we capture the final folded state measured by a structural similarity such as the root-mean squared deviation (RMSD). RMSD measures the average distance between the atoms, the reference (folded) structure and a simulated structure. Other use cases may include additional quantitative measures (such as free energy of binding, or radius of gyration) as well as metrics that capture agreement between experimental and simulation datasets.

DeepDriveMD allows users to set diverse configuration parameters of the workflow, without having to implement single-point solution applications for each use case. Among the main configuration parameters, users can define: the number of ligands, and the number and type of models to train to drive the simulations of MD. Further, DeepDriveMD enables users to specify arbitrary algorithms for feeding data to ML models, to make inferences via one or more of those models and to subsequently drive MD simulations. DeepDriveMD is agnostic towards how each logical component in Fig. 1 is implemented, how and when data are exchanged among

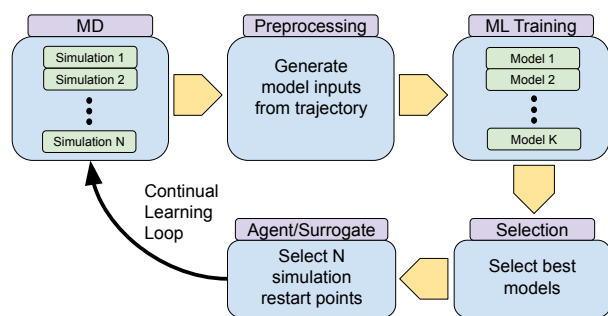


**Figure 1: Computational motif for AI/ML coupled multi-scale MD simulations.**

components, and how and where such data are stored. Users can use arbitrary algorithms to implement each component, including using one or more tasks to implement those algorithms. For example, users may choose to implement a parallel algorithm that scales via MPI or OpenMP, and/or leverage concurrency by implementing a distributed algorithm via multiple independent tasks. Analogously, tasks may store their input/output data into an arbitrary number of files, with the size of each file bounded by the platform capabilities and resource availability. Further, the design space of DeepDriveMD allows for defining arbitrary coordination protocols among its logical components, and mandates nor the degree of concurrency with which those components should be executed, nor the number of instances executed for each type of component.

We present two designs of DeepDriveMD, each supporting a different coordination protocol, and different degrees of concurrency among the tasks implementing the four logical components. In the first design, called DeepDriveMD-F, tasks have input/output dependencies, execute sequentially to satisfy those dependences, and coordinate by writing output files and reading input files. In the second design, called DeepDriveMD-S, tasks execute concurrently, exchanging data while executing, either via network streams or via files that enable concurrent and time-stepped writing/reading operations.

The differences between the design of DeepDriveMD-F and S have profound consequences on how and when data is assumed to be available, how computation is distributed across available resources and, ultimately, how the implementations of those designs perform on HPC resources. For some use cases, data streaming can enable better resource utilization as all the available resources can be used concurrently. Nonetheless, data streaming poses requirements on the task itself as, for example, it has to be coded to produce usable data at runtime, and other tasks need to be able to ingest and use those partial data.

## 4.2 Workflow Engine and Runtime System

DeepDriveMD uses RADICAL-Cybertools (RCT), a package developed to support the execution of heterogeneous workflows and workloads on HPC infrastructures, as workflow engine, runtime system, and batch-systems interface. RCT comprises three components: RADICAL-SAGA (RS) [26], RADICAL-Pilot (RP) [27, 28] and

RADICAL-Ensemble Toolkit (EnTK) [29]. RS is a Python implementation of the Open Grid Forum SAGA standard GFD.90, a high-level interface to distributed infrastructure components like job schedulers, file transfer and resource provisioning services. RS enables interoperability across heterogeneous distributed infrastructures.

RP is a Python implementation of the pilot paradigm and architectural pattern [30]. Pilot systems enable users to submit pilot jobs to computing infrastructures and then use the resources acquired by the pilot to execute one or more workloads. Tasks are executed concurrently and sequentially, depending on the available resources. RP can execute single or multi core tasks within a single compute node, or across multiple nodes. RP isolates the execution of each task into a dedicated process, enabling concurrent execution of heterogeneous tasks.

EnTK is a Python implementation of a workflow engine, designed to support the programming of applications comprised of ensembles of tasks [29]. EnTK executes tasks concurrently or sequentially, depending on their arbitrary priority relation. Tasks are grouped into stages and stages into pipelines, depending on the priority relation among tasks. Tasks without reciprocal priority relations can be grouped into the same stage; tasks that need to be executed before other tasks have to be grouped into different stages. Stages are grouped into pipelines and, in turn, multiple pipelines can be executed either concurrently or sequentially. EnTK uses RP, allowing the execution of workflows with heterogeneous tasks.

In EnTK, tasks are executables, not functions. Task executables are self-contained programs that execute on the operating system of the target HPC platforms. Tasks can be algorithmically heterogeneous, executing simulation, ML training, aggregation, selection and other arbitrary types of operations. Further, tasks may require different types and amounts of resources (e.g., CPU cores, GPUs, amount of ram or file system space), and take different amounts of time to complete their execution. EnTK hides resource acquisition and management, and workflow execution orchestration, allowing users to code arbitrary workflow applications and domain-specific algorithms against its application program interface.

## 4.3 MD and ML implementations

MD simulations are carried out with OpenMM [31] on GPUs. The BBA protein has a total of 505 atoms from 28 residues and is set up with the Amberff99sb-ildn force field [32], using the implicit GBSA-OBC solvation model [33]. The PLpro protein is setup with the Amberff14sb force field [34], using the tip3p water model. The simulation setup has been detailed in Refs. [35, 22]. The solvated PLpro system has  $\sim 132,000$  atoms and 309 residues. The simulations are maintained at 300 K with a Langevin integrator of 2 fs time step and a heat bath friction coefficient of 1. The ligand partial charges are built with Antechamber [36], and atomic interactions are assigned using the General Amber Force Field [37]. The non-bonded interactions are cutoff at 10 Å, calculating the long range interaction with the Particle Mesh Ewald [38]. The PLpro systems are solvated in  $110^3$  Å<sup>3</sup> box with periodic boundary condition. Each simulation reports a configuration every 50 ps.

Currently, we support two prototypical unsupervised generative ML models: a convolutional variational autoencoder (CVAE) [39] written in Keras/TensorFlow 2.1.2 [40, 41], and a 3D adversarial autoencoder (3dAAE) [4] written in PyTorch 1.6.0 [42]. Both models

automatically reduce the high dimensional MD trajectory data into a latent vector representation in which similar energetic and structural states are clustered together.

The CVAE views the MD trajectory as a contact matrix of  $C^\alpha$  atoms (within 8 Å cut-off) at each frame, and learns to represent this matrix in a latent space [39]. The model architecture consists of a symmetric encoder/decoder pair with 4 convolutional layers, each with 64 filters, and a stride of 2 in the second layer followed by a single linear layer of 128 neurons and dropout of 0.25. The latent space is fixed at 10 dimensions and the decoder, composed of transposed convolution operators, reconstructs the input contact matrix. We defined the loss function as the sum of the binary cross entropy reconstruction and KL divergence to an isotropic gaussian prior  $\mathcal{N}(0, 1)$ . This loss function is optimized using RMSprop with learning rate 0.001,  $\rho = 0.9$ , and  $\epsilon = 1e - 08$ . The CVAE model is implemented in both the DeepDriveMD-F/S frameworks; the mode of execution however may vary (sequential/file-system vs. streaming versions).

Similar to CVAE, the 3D-adversarial autoencoder (3dAAE) also makes use of an encoder/decoder pair, but instead of using KL divergence to incorporate a prior, it uses an additional discriminator network which is jointly optimized [4]. We find 3dAAE to be a more appropriate choice for larger systems since it views the MD trajectory as a sequence of  $C^\alpha$  atomic positions in a Cartesian space with shape  $3 \times N$ , versus the quadratic  $N^2$  contact matrices. To train the network, we optimize a chamfer distance reconstruction loss and a Wasserstein adversarial loss with gradient penalty. In general, point clouds do not have a canonical ordering, however, in the case of protein modeling, the amino acid sequence defines a natural ordering of the atoms. We opted to use the same architecture and learning hyperparameters as in Ref. [4], replacing the Adam optimizer with RMSprop. We used this ML model to understand the protein-ligand interactions in UC2.

In order to search for undersampled regions of the conformational space, we use traditional outlier detection methods on the latent vectors produced by the generative models. Since the CVAE tends to form well defined clusters, we found it best to use Density-Based Spatial Clustering of Applications with Noise (DBSCAN) [43] implemented in scikit-learn [44] to discover points outside the main clusters. As a result of the adversarial training, 3dAAE has a smoother latent space. To discern outliers in the 3dAAE latent space, we use Local Outlier Factor (LOF) [45] implemented in RAPIDS [46] which measures local deviation using the k-nearest latent vectors.

## 4.4 DeepDriveMD Implementations

Both DeepDriveMD-F and DeepDriveMD-S use the RCT tools and the same MD engine and ML models. Their main differences are in the tasks they use to implement the logical components of Fig. 1, the degree of concurrency with which they execute those tasks and the way tasks exchange data at runtime.

**4.4.1 DeepDriveMD-F.** DeepDriveMD-F uses a single EnTK Pipeline which orchestrates the execution and I/O dependencies of the learning loop. The pipeline contains 4 EnTK Stages: MD, Preprocess, ML training, Selection, and Agent in Fig. 2. Each Stage executes serially, spawning at least one EnTK Task which receives input from upstream tasks and writes its output to disk. The five Stages

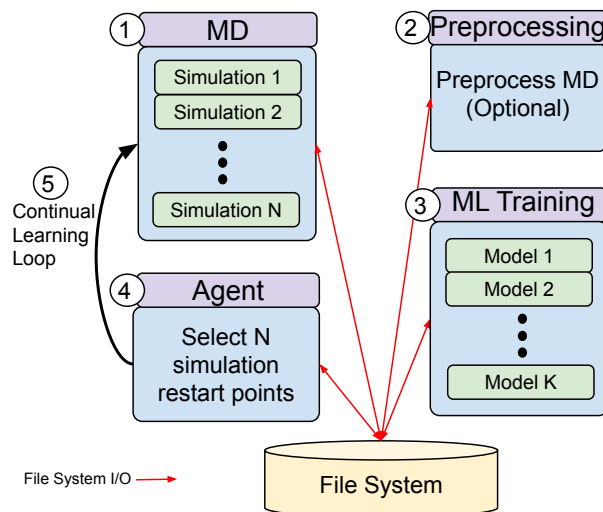


**Figure 2: DeepDriveMD-F architecture. Circled numbers indicate the order of components execution. In blue are EnTK stages; green are EnTK tasks.**

repeat in a loop until some conditions on the simulation space or a given objective are met.

To create a uniform interface between Stages, DeepDriveMD-F uses a single YAML configuration file containing both system- and task-level parameters. The YAML configuration is parsed, typed, and validated using Pydantic [47], enabling on-the-fly generation of task configuration files. In that way, users can develop arbitrary task code and pass the necessary parameters via the YAML configuration file. In turn, DeepDriveMD-F uses a `-c` argument for each task's executable to receive the YAML file. To further abstract the code from the specifics of each target HPC platform, users are required to include stage-level parameters in the input YAML file, such as `pre_exec` commands, the executable to run, executable's arguments, and hardware requirements for each task.

On start, DeepDriveMD-F creates an experiment root directory and a subdirectory for each stage. At the beginning of each pipeline iteration, a stage directory labeled with the iteration is created in each of the stage subdirectories. Task directories are also created within each of the stage directories for each task specified in the YAML configuration. DeepDriveMD-F then writes the YAML file for each task to the task's directory and, finally, the stages and tasks are executed using EnTK.

The first stage (MD) runs a user-specified number of MD simulation tasks in parallel and the flexibility of the framework allows for the use of an arbitrary simulation engine. When using the OpenMM [31] engine, we take advantage of its reporter mechanism, preprocessing each frame of the simulation on the fly to a format that can be inputted into the chosen ML model. We write the preprocessed data into an HDF5 [48] file and the raw simulation data to a DCD file at the end of the MD stage. This avoids I/O bottlenecks by processing the simulation data while it's still in memory into a much smaller dataset stored in the HDF5 file. Once the MD stage finishes, an optional Preprocessing stage runs. This enables

the use of simulation engines without a reporter mechanism by allowing arbitrary preprocessing of the simulation output files.

Once the simulation data is preprocessed, the ML stage retrieves the resulting datasets for training. The ML stage allows for arbitrary ML algorithms to be run on one or several CPU/GPUs, allowing for both data and model parallelism to train a deep neural network. The ML stage can be configured to train for more epochs on the first iteration, fewer epochs in following iterations, and can optionally skip training on selected iterations. In addition, a pretrained model can be used to initialize the weights, which can accelerate the ML stage by avoiding the need to train a model from scratch.

After the ML stage, the model selection stage selects the model weights to use during inference. In principle, one could specify any model selection criterion, e.g., the most accurate model. In practice, we simply select the most recent weights outputted by the ML stage.

The final stage acts as an agent which selects the portions of simulation space to sample in order to further explore the space or optimize a given objective. The Agent stage receives the model weights and HDF5 files from the latest iteration of the DeepDriveMD-F pipeline, as well as an arbitrary selection of previous HDF5 files. Then, it searches the data for the points that would optimize a user specified objective when restarting the simulation. In its current form, the Agent stage consists of an outlier detection routine which runs on a generative models latent space. This unsupervised criterion can be optionally augmented with domain-specific objectives, e.g., in the protein folding use case, minimizing the RMSD between the current and folded structure. Once the outliers are selected, a JSON file is written containing metadata about the outlying frames of the simulations. This file is subsequently read by each MD task to initialize the next round of MD simulations.

**4.4.2 DeepDriveMD-S.** As illustrated in Fig. 3, DeepDriveMD-S runs all logical components (Simulation, Aggregation, ML Training, Agent) continuously and in parallel, exchanging data using the Adaptable Input/Output System (ADIOS) [49]. Data exchanges use either the network (*Simulation to Aggregator*) or ADIOS BP files (*Aggregator to ML Training*; *Aggregator to Agent*).

ADIOS allows for exchanging data between producer and consumer via either network or ADIOS BP files. The application deals with streams and needs not to know if data are written to or read from network or a file. This is configured in an XML file. ADIOS has a notion of time steps which allows, for example, for blocking or non-blocking communication via network. BP is a native ADIOS output format similar to HDF5 and convertible to HDF5.

EnTK acquires the requested resources and launches RADICAL-Pilot which pulls the tasks specified via DeepDriveMD-S and then executes them all concurrently as the amount of requested resources allows for maximal execution concurrency.

Instead of one EnTK Pipeline with four sequential Stages, DeepDriveMD-S uses four parallel pipelines, each with one Stage to allow parallel execution of all the tasks. The MD Simulation Pipeline and the Aggregator Pipeline concurrently execute multiple Simulation and Aggregator tasks respectively. Simulation tasks are partitioned, and each partition is assigned to an Aggregator task. Each Aggregator continuously collects data from its subset of simulations, simultaneously evaluating from each simulation some physical observables. In this way, an Aggregator could stop and replace a

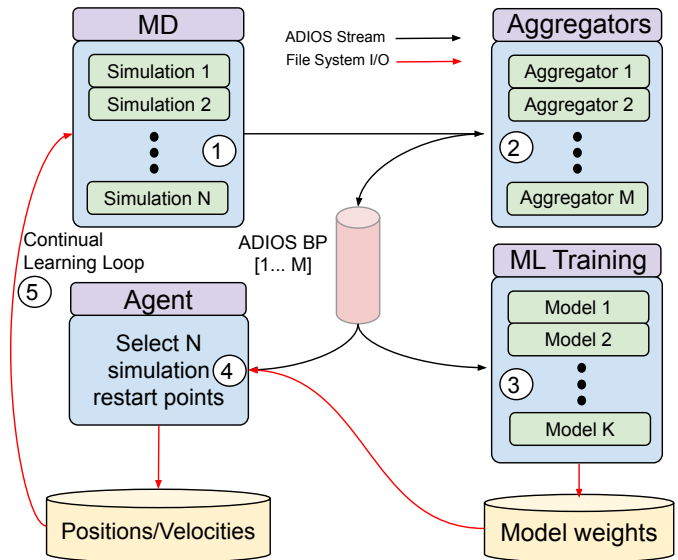


**Figure 3: DeepDriveMD-S architecture.** Circled numbers indicate the data flow. In purple are DeepDriveMD-S components; blue are EnTK pipelines which; green are EnTK Tasks; red is the ADIOS BP stream; yellow is the file system. Pipelines and tasks run concurrently.

simulation that is no longer producing relevant results. The ML Pipeline uses data from the Aggregators to train the CVAE, and the Agent Pipeline uses data from this Aggregator and ML tasks to derive the initial configuration of new simulation tasks.

Each MD simulation continuously sends data to its aggregator via the network, using ADIOS. Each aggregator collects data from its subset of simulations and saves them to a single ADIOS BP file. We configure ADIOS network data exchange to be blocking: MD simulation cannot write to an ADIOS stream until the aggregator picks up the data. For performance reasons, a buffer of 50,000 elements is used between a simulation and an aggregator.

Each task has its own independent infinite loop of iterations. There is no global loop that coordinates tasks but just a partial synchronization among different types of tasks, via ADIOS blocking or via file locking. At each iteration, the ML and Agent tasks read from the aggregators' BP files only the new data produced since the last iteration. All the necessary old data is kept in memory since a task never stops until the end of the workflow execution. We use here streaming via files and not via the network, as we did between simulations and aggregators, because we want to save the reported states for possible subsequent analysis. However, if all the analysis were done online, we could configure ADIOS to stream via network between the ML and Agent tasks as well. That would require a small change to the ADIOS XML configuration file and not to the DeepDriveMD-S implementation.

Once one ML task finishes training, the best model – evaluated in terms of validation loss – is moved from a temporary directory to a directory checked by the Agent task. The next training iteration starts immediately, using the weights from the previous iteration as an initial condition and utilizing all the available data, including

those accumulated in the previous iteration. If necessary, the ML Task can use the last  $N$  reported states from each aggregator instead of using all the reported states.

The Agent task uses up to 80,000 recently reported conformations and selects outliers based on the DBSCAN approach. The RMSD between the folded state and the outliers are computed and stored in a Python pickle object, serving as an outlier catalog from which simulations randomly pick up the next initial state. To avoid race conditions, the access to the pickled class is file-locked for the Agent and Simulations tasks. While an iteration is running, the outliers and catalog files are written into a temporary directory and, only at the end of an iteration, the files are moved into the directory which is checked by the simulation Tasks. Also in this case, the moving operation is file-locked to avoid race conditions.

## 5 SCIENTIFIC VALIDATION

In light of the methodological novelty of ML-driven ensemble simulations, we assess the biophysical (scientific) validity of results, in addition to the performance enhancement.

### 5.1 Validation

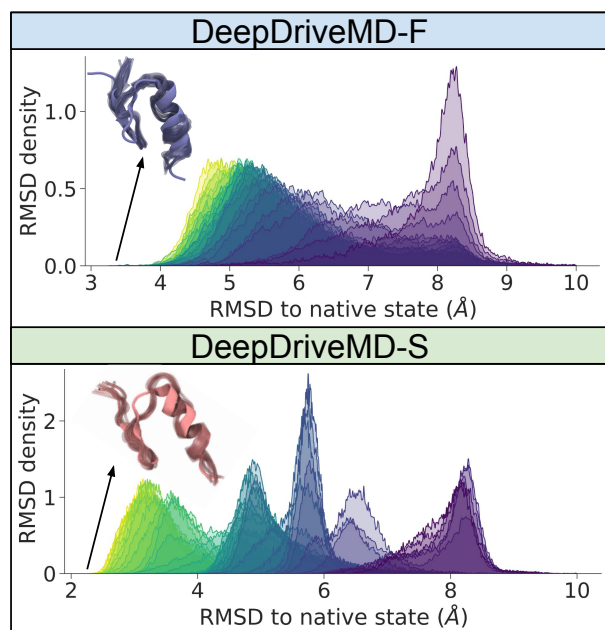


**Figure 4:** Comparing BBA folding pathways via RMSD evolution over each iteration of DeepDriveMD (progressing from purple/early iterations to yellow/late iterations). Both implementations observe a distribution shift towards smaller RMSD values, indicative of BBA folding. The folded ensemble sampled by the respective simulations are shown in a cartoon representation (transparent colors) and compared to the folded state (solid color). Although the RMSD histograms are different, both approaches converge towards the folded state eventually, achieving 3.28 Å for DeepDriveMD-F versus 2.25 Å for DeepDriveMD-S.

For UC1, we measure the convergence to the folded state, or how well we can access the final folded state(s) of the protein as determined with structural biology experimental techniques, e.g., X-ray crystallography or nuclear magnetic resonance. As the ML progressively learns a latent representation (based on the CVAE) and guides the selection of conformations to be simulated next through successive iterations, we posit that the RMSD of the selected conformations (as part of the agent) must progress towards lower RMSDs. Hence we plot a histogram of the RMSDs from the Agent stage of the simulations with a color scheme corresponding to the successive iterations of our continual learning loop, where blue represents earlier iterations and subsequent iterations progress towards green and yellow colors. As shown in Fig. 4, both DeepDriveMD-F/S sample lower RMSD states. Despite a slight difference in the RMSDs, both folded ensembles, shown in blue (DeepDriveMD-F) and orange (DeepDriveMD-S), depict considerable agreement in terms of the formation of secondary structural features such as the core  $\alpha$ -helix and more flexible  $\beta$  sheet, with respect to the final folded state of the protein (solid colors). This entails that both approaches can indeed result in valid sampling of the final folded state of BBA.

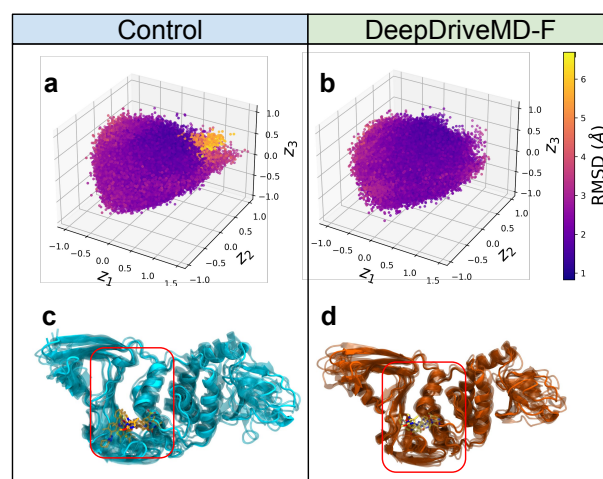


**Figure 5:** Principal components of the adversarial autoencoder embeddings of (a) control MD simulations and (b) DeepDriveMD-F, painted by RMSD of each conformation from the respective simulations shows clustering of conformational states. A subset of conformations sampled uniformly across the RMSD histograms are shown in a cartoon representation (along with the ligand shown as sticks in yellow) for (c) control and (d) DeepDriveMD-F simulations. Our ML-driven approach picks up stabilization of PL-Pro’s primary binding pocket in contrast to the control simulations, which shows larger fluctuations in the same area (highlighted as red rounded rectangles).

For UC2, we compare the learned representations between the control simulations (no ML) vs. DeepDriveMD-F. The 64 dimensional latent space summarized from the simulations can be projected using principal component analysis (PCA) to visualize the top

three dimensions of the control (Fig. 5.a) and for the DeepDriveMD-F (Fig. 5.c) simulations. It is important to note that the objective of the PLC simulations is different than in UC1, where the criterion for selection of the states is based on the stability of how well the ligand interacts with the protein active site. Hence the selection strategy ‘rewards’ the ligands that stabilize the protein, in contrast to a plain MD simulation which does not pay any attention to ligand stability. Confirming this, one can observe that the RMSD distribution in the control simulations are significantly larger (varying between 0.85 Å to 6.85 Å) than the DeepDriveMD-F simulations (0.85 Å to 4.6 Å). A subset of conformations drawn from the distribution of the control simulations (Fig. 5.b) and DeepDriveMD-F (Fig. 5.d) depict significant fluctuations in PLPro’s ligand-binding pocket for the control simulations compared to the DeepDriveMD-F simulations (indicated by rounded red rectangles).

## 5.2 Scientific Performance

We measure the *sampling effectiveness* by using the fraction of the total population explored – with and without ML approaches – as a function of time [50]. To achieve this, we selected the states sampled at some time and compare it against all states obtained with respect to reference simulations. For UC1, we compare our simulations to long timescale simulations of the FSD-EY (BBA) system ( $O(100\mu s)$ ) using the Anton-1 hardware, providing extensive information on all possible states sampled for its folding process [25]. The conformers from the three simulations (DeepDriveMD-F/S and Anton-1 run of  $102\mu s$ ) are used to train a CVAE network with a 10 dimension latent space. The embeddings are then clustered with MiniBatchKmeans, with  $k = 100$ . This set up allows us to compare the states sampled by each simulation, while keeping a consistent definition of the conformational states sampled in the simulations. In Fig. 6, the ratio of sampled states in a simulation at certain time  $T$  is defined as how many clusters the simulation has traversed before  $T$  divided by total number of states (100).

Fig. 6 indicates that ML-driven methods enhance sampling from  $O(10)$  to  $O(100)$ . As the red arrow indicates in Fig. 6, it takes the ML-driven ensemble  $\sim 18$  ns to cover 50% of conformational states covered, while the Anton-1 simulation takes nearly  $1.69 \mu s$ . Compared to UC3 in Ref. [4] where a (lower bound) performance improvement of  $O(10)$  was reported, one can reasonably conclude at least an order of magnitude speedup with DeepDriveMD simulations.

## 6 PERFORMANCE CHARACTERIZATION

We use the two use cases outlined to measure the performance of the two implementations of DeepDriveMD described in §4: the protein ligand complex (PLC) use case (UC2) for DeepDriveMD-F, and the protein folding use case (UC1) for comparing DeepDriveMD-F and DeepDriveMD-S. In each case, we measure performance for different numbers of ligands and proteins to fold.

### 6.1 DeepDriveMD-F performance

Table 1 shows the parameters used for the PLC use case experiments. Those experiments show the scaling behavior of DeepDriveMD when varying four configuration parameters: (1) the HPC platform used for the experiments; (2) the number of ligands; (3) the number of tasks executed; and (4) the amount of resources requested. All the

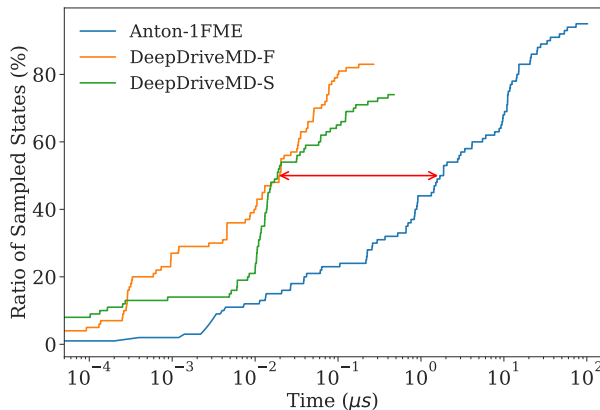


**Figure 6: Comparing the sampling efficiency of DeepDriveMD-F and DeepDriveMD-S with long time-scale simulations using Anton-1 for FSD-EY folding.**

**Table 1: Configuration & overhead, PLC-1–7 experiments.**

| Exp.  | Ligands | Nodes | Tasks | Platform | Overhead |
|-------|---------|-------|-------|----------|----------|
| PLC-1 | 1       | 20    | 250   | Summit   | 334.21s  |
| PLC-2 | 1       | 30    | 250   | Lassen   | 302.34s  |
| PLC-3 | 8       | 160   | 2000  | Summit   | 265.05s  |
| PLC-4 | 8       | 240   | 960   | Lassen   | 314.83s  |
| PLC-5 | 51      | 1020  | 6120  | Summit   | 254.01s  |
| PLC-6 | 120     | 20    | 120   | Summit   | 325.84s  |
| PLC-7 | 960     | 240   | 960   | Summit   | 375.98s  |

experiments measure how overheads and resource utilization vary as a function of different values for those configuration parameters.

Experiments PLC-1–4 evaluate between one and eight ligands, using between 20 and 160 compute nodes on Summit, and 30 and 240 nodes on Lassen. Experiment PLC-5 evaluates 51 ligands, using 1020 compute nodes on Summit, while experiments PLC-6–7 uses 20 and 240 to evaluate 120 and 960 ligands on Summit. The amount of data aggregated by the aggregation stage increases with the number of simulations and, as a consequence, the amount of data on which to train the ML models also increases.

In experiments PLC-1–7, overhead indicates all the time spent not executing any workflow task when resources are available. It includes the time taken by DeepDriveMD and RADICAL-Cybertools to resolve the tasks dependences, prepare the execution environment and submit the tasks for execution. Overhead is relatively invariant of the number of ligands analyzed, averaging  $\sim 310$  seconds across the PLC experiments. PLC-1–7 have different total execution times, indicating that overheads are also invariant of the time taken by all the workflow tasks to execute. Finally, overheads are invariant across HPC platforms as their value are comparable between Summit and Lassen. Together, those invariances show that the scaling behavior of DeepDriveMD-F is decoupled from the configuration of the use cases it supports, the time taken to execute the workflows and the HPC platform on which it executes.



Note that we reduced the total time taken to execute all workflow tasks so as to reduce allocation usage. With UC2, DeepDriveMD-F would run for ~12 hours in production, making the mean 310 seconds of overhead insignificant for resource usage considerations.

Fig. 7 shows some relevant difference in resource utilization for experiments PLC-2, 4, 5 and 7 — the plots of PLC-1, 3 and 6 are similar to those we show in the figure. The purple boxes indicate the resources used by each workflow task over time while the white space indicates either resources not required by the tasks (e.g., GPU-only tasks do not require the available CPU cores), or resources that DeepDrive-F was not able to use due to the time taken to schedule, place and launch the tasks.

We annotated Fig. 7a to show the types of tasks being executed. First *Simulation* tasks execute concurrently on all GPUs (Fig. 7a, red box); then a *Preprocessing* task runs on enough CPUs to balance parallelism and communication overhead (Fig. 7a, blue box); then three *ML Training* tasks execute on three GPUs (Fig. 7a, green box); and finally a large *MPI Agent* task executes on all CPUs and GPUs (Fig. 7a, black box). In the PLC experiments, this cycle repeats twice to limit resource consumption, but in production runs the cycle may repeat up to tens of times until convergence is reached.

The disparity between the duration of the *Simulation* tasks and that of the other tasks allows DeepDriveMD-F to be relatively efficient despite executing each stage sequentially. Nonetheless, resource utilization decreases with the scale of the workflow executed due to the time taken to schedule an increasing number of tasks on an increasing number of resources. This is best showed by comparing Fig. 7a and Fig. 7c. In the latter, scheduling time accumulates, determining a shift to the right of all the tasks, ultimately increasing execution time and reducing resource utilization. Note that this is different from the overheads reported above, as the overhead metric takes into account only the time in which no task is executing but resources are available.

Ultimately, Fig. 7 shows that, in order to reach better resource utilization, DeepDriveMD might have to use a task coordination protocol that enables higher concurrency among tasks. In that way, as soon as the first MD task execution ends, its data could be processed without waiting for all other MD tasks to terminate. Further, improvement of resource utilization could be achieved by enabling data to be processed while MD simulations are still executing. Both those capabilities are implemented by DeepDriveMD-S.

## 6.2 DeepDriveMD Performance: F vs. S

Table 2 shows the parameters used for the UC1 experiments. These experiments measure the scaling behavior of DeepDriveMD-F and DeepDriveMD-S on LLNL Lassen, when folding the BBA protein on 30 and 33 compute nodes respectively. Measuring overheads and resource utilization for both experiments, enables a direct comparison between the performance of the file- and streaming-based coordination patterns for UC1.

As described in §4, DeepDriveMD-S uses streaming communication among tasks to enable more efficient workflow execution via increased concurrency and to reduce the potential of I/O bottlenecks caused by writing intermediate files in numbers that grows proportionally with the number of tasks executed concurrently. For example, in the PLC use case, each simulation tasks write both

intermediate HDF5 and trajectory files, creating a pressure on the network filesystem that increases with the number of concurrent MD simulation executed.

The performance of DeepDriveMD-F and DeepDriveMD-S are compared when folding BBA protein. In the simulation stage of both implementations, 120 MD simulation tasks are running in parallel. However, as one can see from Fig. 8, in DeepDriveMD-S simulations run continuously without gaps while in DeepDriveMD-F a simulation stage is followed sequentially by ML stage (every other iteration) and the Agent stage (as already seen in Fig. 7). This allows DeepDriveMD-S to perform 1.6 times more simulations per unit of time than DeepDriveMD-F (orange bars in Fig. 8).

DeepDriveMD-S also executed more ML Training, and Agent tasks than did DeepDriveMD-F. While DeepDriveMD-F avoids executing Aggregation tasks, Fig. 8 clearly shows how DeepDriveMD-S executes many more ML Training tasks (Fig. 8 red) and Agent tasks (Fig. 8 green). This is because DeepDriveMD-S enables the analysis of partial simulation data while simulations are executing, further speeding up the execution of the overall workflow compared to DeepDriveMD-F.

From a resource utilization perspective, DeepDriveMD-S utilizes the computing resources allocated via EnTK more effectively while the sequential Stages of DeepDriveMD-F use a lower amount of resources, periodically leaving some of the nodes idle. For example, to implement UC1, DeepDriveMD-F concurrently executes 120 Simulation tasks, utilizing 120 GPUs but the ML Training task utilizes only 1 GPU, leaving the rest of the available GPUs idling. Further, DeepDriveMD-S avoids saving intermediate data to disk, using ADIOS as described in §4. For UC1, DeepDriveMD-S avoids writing ~50GB to disk by streaming them across the concurrently executing tasks. This will be especially important for use cases like UC3, where data from large simulations across  $O(100)$  nodes would create a I/O bottleneck without streaming capabilities.

We estimate the overall percentage of time spent on ADIOS I/O by adding ADIOS I/O times from all the tasks and dividing it by total wall time for all the tasks: 0.8%. However, most of this time is hidden from the end user due to the fact that the components run concurrently. The only thing that the end user would really see is the ADIOS overhead in simulations which is 0.3%. The performance of the other components might affect the speed of convergence but not the total number of executed simulations.

## 7 CONCLUSIONS

AI/ML methods have an increasingly visible and important role in smarter computational campaigns and accelerating scientific discovery. The main reason for the success of such techniques is that they offer simple, scalable and fairly general means to deal with high-dimensional, potentially high volume and velocity of scientific datasets. Bio-molecular simulations necessitates the use of AI/ML techniques to automatically analyze such datasets, and to guide ensembles of HPC bio-molecular simulations through a high-dimensional search-space effectively and efficiently.

We identify a general computational motif coupling AI/ML to HPC simulation ensembles, and implement DeepDriveMD — an application framework to support a variety of AI-driven simulations

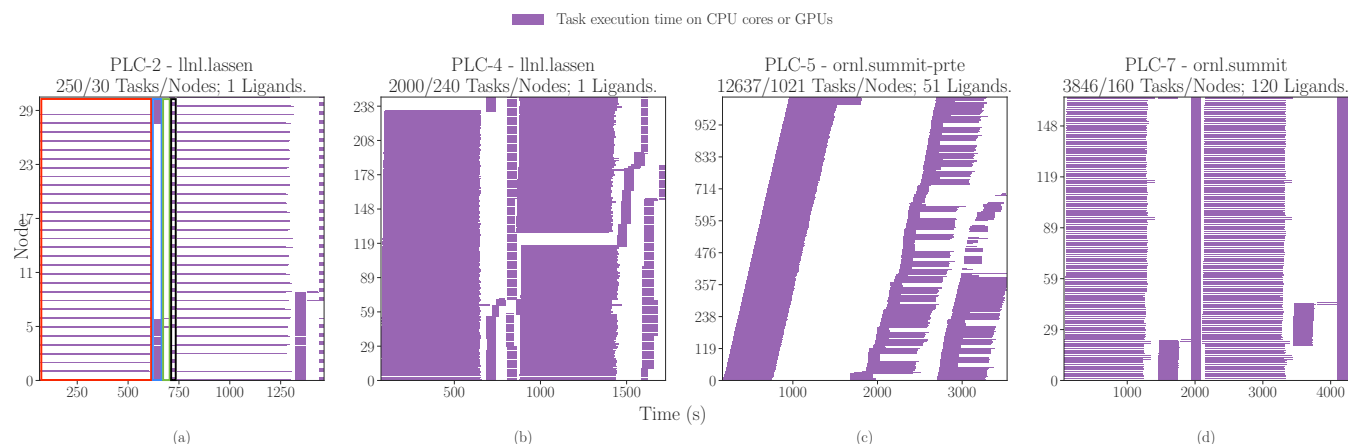


**Figure 7: Task execution on HPC compute nodes over time. Purple indicates when a compute node is occupied by a task. Red, blue, green and black squares in (a) indicate different stages of the workflow executed by DeepDriveMD-F: MD simulation, Preprocessing, ML Training and Agent.**

**Table 2: Performance and resource utilization for DeepDrive-F/S on Lassen. 30/33 nodes are used for 120 MD tasks.**

| System        | 10ns Simulation Task |          |          |           | Aggregator Task |          |          |
|---------------|----------------------|----------|----------|-----------|-----------------|----------|----------|
|               | duration             | #iter./h | #CPU;GPU | #instance | duration        | #iter./h | #CPU;GPU |
| DeepDriveMD-F | 591 s                | 3.9      | 1; 1     | N/A       | N/A             | N/A      | N/A      |
| DeepDriveMD-S | 576 s                | 6.1      | 1; 1     | 10        | 3.2 s           | 1091     | 1; 0     |

| System        | ML Task  |          |          |                |         |
|---------------|----------|----------|----------|----------------|---------|
|               | duration | #iter./h | #CPU;GPU | #samples/iter. | #epochs |
| DeepDriveMD-F | 282 s    | 2        | 1; 1     | 24,000; 48,000 | 15; 20  |
| DeepDriveMD-S | 393 s    | 9.2      | 1; 1     | 80,000         | 20      |

| System        | Agent Task |          |          |                |           |
|---------------|------------|----------|----------|----------------|-----------|
|               | duration   | #iter./h | #CPU;GPU | #samples/iter. | #outliers |
| DeepDriveMD-F | 111 s      | 3.7      | 1; 1     | 24,000; 48,000 | 500–700   |
| DeepDriveMD-S | 116 s      | 31       | 39; 1    | <80,000        | 4000–4500 |

scenarios. We evaluated the design, implementation, and performance of DeepDriveMD, and demonstrate that by driving ensembles of MD simulations with AI/ML approaches, one can expect to easily achieve 1-2 orders of magnitude improvement in time-to-solution, while covering the same conformational landscape as quantified by the states sampled during the actual simulation.

Motivated by the potential scientific impact and applicability to a range of physical systems, we evaluated two distinct design paradigms of coupling AI/ML with HPC simulation ensembles — *sequential* (DeepDriveMD-F), and *streaming* (DeepDriveMD-S). While both approaches provide similar scientific end points (i.e., in UC1, they resulted in sampling similar folded states with well defined secondary structural features), the learning strategy (streaming vs. sequential) offers unique takeaways. The streaming approach lets us run more simulations per unit time (at least 1.6x) and offers

better resource utilization just because the various jobs can be run in parallel and continuously.

DeepDriveMD-F provides biophysically relevant insights into conformational landscapes of complex bio-molecular systems as observed in Fig. 5 for UC2 and as seen in UC3 [4]. As a baseline from UC1, DeepDriveMD provides at least O(10-100) speedup in time-to-solution for conventional MD simulations. It must be noted here that we used a single starting structure (with different velocity initialization) for our ensemble simulations; we expect that with a diverse pool of starting structures (with random velocity initialization) this speedup would be only further accelerated. Although we used different force-fields for modeling the individual use cases, a systematic evaluation across diverse force-field and initial condition remains to be evaluated.

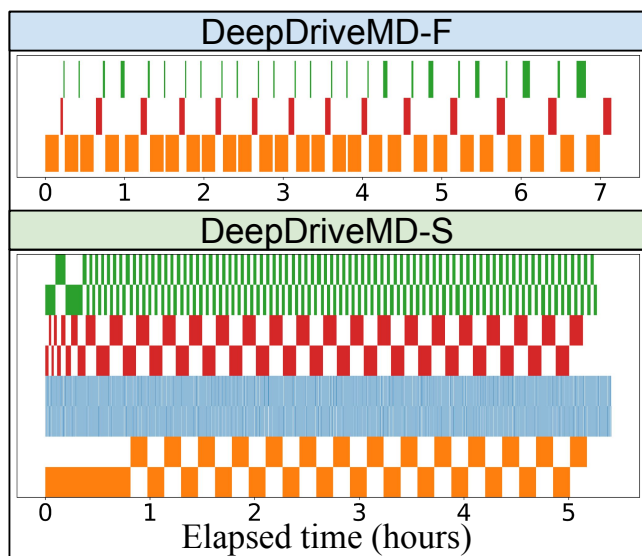


**Figure 8: Timeline of task execution when running the UC1 on Lassen.** Each bar corresponds to one iteration of: Simulation task (orange); Aggregation task (blue); ML Training task (red), Agent task (green). DeepDriveMD-F runs ML after every other simulation while DeepDriveMD-S runs different types of iterations independently and without gaps. In DeepDriveMD-S, every second iteration is shown on a different line, allowing to distinguish between different iterations. Only 1 out of 120 Simulation tasks and 1 out of 10 Aggregation tasks are shown to make the diagram readable.

Additionally, the runtime behaviors of DeepDriveMD-F and DeepDriveMD-S suggest that these implementations may have specific application contexts under which each one may be more relevant. In particular, with simulations guided by reinforcement/active learning strategies [9], DeepDriveMD-S can achieve better performance whereas for approaches that utilize a static learning process (e.g., learning force-field parameters [51]), DeepDriveMD-F may be more appropriate. Of course, effectively combining the streaming and sequential workflows to support broader range of use cases (e.g., data-driven multiscaling [3]) would be future extensions to this paper. Finally, the integration of our workflow(s) with heterogeneous AI accelerators offers exciting avenues for further development.

**Acknowledgements** This work is supported by ECP Projects: CANDLE, CODAR and ExaWorks. This research used resources at the Oak Ridge Leadership Computing Facility at the Oak Ridge National Laboratory, which is supported by the Office of Science of the U.S. Department of Energy under Contract No. DE-AC05-00OR22725. Anda Trifan acknowledges support from the United States Department of Energy through the Computational Sciences Graduate Fellowship (DOE CSGF) under grant number: DE-SC0019323.

## REFERENCES

- [1] Vivek Balasubramanian et al. “Adaptive ensemble biomolecular applications at scale”. In: *SN Computer Science* 1.2 (2020), pp. 1–15.
- [2] Peter M Kasson and Shantenu Jha. “Adaptive ensemble simulations of biomolecules”. In: *Current Opinion in Structural Biology* 52 (2018). Cryo electron microscopy: the impact of the cryo-EM revolution in biology • Biophysical methods, pp. 87–94. ISSN: 0959-440X. DOI: <https://doi.org/10.1016/j.sbi.2018.09.005>. URL: <http://www.sciencedirect.com/science/article/pii/S0959440X1830085X>.
- [3] Francesco Di Natale et al. “A massively parallel infrastructure for adaptive multiscale simulations: modeling RAS initiation pathway for cancer”. In: *Proceedings of the International Conference for High Performance Computing, Networking, Storage and Analysis*. 2019, pp. 1–16.
- [4] Lorenzo Casalino et al. “AI-Driven Multiscale Simulations Illuminate Mechanisms of SARS-CoV-2 Spike Dynamics”. In: *bioRxiv* (2020). DOI: 10.1101/2020.11.19.390187. eprint: <https://www.biorxiv.org/content/early/2020/11/20/2020.11.19.390187.full.pdf>. URL: <https://www.biorxiv.org/content/early/2020/11/20/2020.11.19.390187>.
- [5] Geoffrey Fox et al. “Learning everywhere: Pervasive machine learning for effective high-performance computation”. In: *2019 IEEE International Parallel and Distributed Processing Symposium Workshops (IPDPSW)*. IEEE, 2019, pp. 422–429.
- [6] Shantenu Jha and Geoffrey Fox. “Understanding ML Driven HPC: Applications and Infrastructure”. In: *15th International Conference on eScience*. IEEE, 2019, pp. 421–427.
- [7] Geoffrey Fox and Shantenu Jha. “Learning Everywhere: A Taxonomy for the Integration of Machine Learning and Simulations”. In: *2019 15th International Conference on eScience (eScience)*. <https://arxiv.org/abs/1909.13340>. IEEE, 2019, pp. 439–448.
- [8] Rafael C. Bernardi, Marcelo C.R. Melo, and Klaus Schulten. “Enhanced sampling techniques in molecular dynamics simulations of biological systems”. In: *Biochimica et Biophysica Acta (BBA) - General Subjects* 1850.5 (2015). Recent developments of molecular dynamics, pp. 872–877. ISSN: 0304-4165. DOI: <https://doi.org/10.1016/j.bbagen.2014.10.019>. URL: <https://www.sciencedirect.com/science/article/pii/S0304416514003559>.
- [9] João Marcelo Lamim Ribeiro et al. “Reweighted autoencoded variational Bayes for enhanced sampling (RAVE)”. In: *The Journal of Chemical Physics* 149.7 (2018), p. 072301. DOI: 10.1063/1.5025487. eprint: <https://doi.org/10.1063/1.5025487>. URL: <https://doi.org/10.1063/1.5025487>.
- [10] Jakub Ryzewski and Omar Valsson. *Multiscale reweighted stochastic embedding (MRSE): Deep learning of collective variables for enhanced sampling*. 2020. arXiv: 2007.06377.
- [11] Luigi Bonati, Yue-Yu Zhang, and Michele Parrinello. “Neural networks-based variationally enhanced sampling”. In: *Proceedings of the National Academy of Sciences* 116.36 (2019), pp. 17641–17647. ISSN: 0027-8424. DOI: 10.1073/pnas.1907975116. eprint: <https://www.pnas.org/content/116/36/17641.full.pdf>. URL: <https://www.pnas.org/content/116/36/17641>.

- [12] Carlos X. Hernández et al. “Variational encoding of complex dynamics”. In: *Phys. Rev. E* 97 (6 June 2018), p. 062412. doi: 10.1103/PhysRevE.97.062412. url: <https://link.aps.org/doi/10.1103/PhysRevE.97.062412>.
- [13] Hendrik Jung, Roberto Covino, and Gerhard Hummer. *Artificial Intelligence Assists Discovery of Reaction Coordinates and Mechanisms from Molecular Dynamics Simulations*. 2019. arXiv: 1901.04595 [physics.chem-ph].
- [14] Arvind Ramanathan et al. “Artificial intelligence techniques for integrative structural biology of intrinsically disordered proteins”. In: *Current Opinion in Structural Biology* 66 (2021), pp. 216–224. issn: 0959-440X. doi: <https://doi.org/10.1016/j.sbi.2020.12.001>. url: <https://www.sciencedirect.com/science/article/pii/S0959440X20302190>.
- [15] Maria Korshunova et al. “OpenChem: A Deep Learning Toolkit for Computational Chemistry and Drug Design”. In: *Journal of Chemical Information and Modeling* 61.1 (2021), pp. 7–13.
- [16] Stefan Doerr et al. “TorchMD: A Deep Learning Framework for Molecular Simulations”. In: *Journal of Chemical Theory and Computation* (Mar. 2021). issn: 1549-9626. doi: 10.1021/acs.jctc.0c01343. url: <http://dx.doi.org/10.1021/acs.jctc.0c01343>.
- [17] Bharath Ramsundar et al. *Deep Learning for the Life Sciences*. <https://www.amazon.com/Deep-Learning-Life-Sciences-Microscopy/dp/1492039837>. O’Reilly Media, 2019.
- [18] Cray/HPE. *SmartSim Infrastructure Library*. url: <https://github.com/CrayLabs/SmartSim>. (accessed: 04.09.2021).
- [19] Oliver Hennigh et al. “NVIDIA SimNet<sup>TM</sup>: an AI-accelerated multi-physics simulation framework”. In: *arXiv preprint arXiv:2012.07938* (2020).
- [20] Sam Ade Jacobs et al. “Enabling Rapid COVID-19 Small Molecule Drug Design Through Scalable Deep Learning of Generative Models”. In: *International Journal of High Performance Computing Applications* (2021). url: [https://sc20.supercomputing.org/proceedings/tech\\_paper/tech\\_paper\\_pages/cov101.html](https://sc20.supercomputing.org/proceedings/tech_paper/tech_paper_pages/cov101.html).
- [21] Jens Glaser et al. “High-throughput virtual laboratory for drug discovery using massive datasets”. In: *The International Journal of High Performance Computing Applications* (2021), p. 10943420211001565.
- [22] Aymen Al Saadi et al. “IMPECCABLE: Integrated Modeling PipelinE for COVID Cure by Assessing Better LEads”. In: *arXiv preprint arXiv:2010.06574* (2020). <https://arxiv.org/abs/2010.06574>.
- [23] Christoph Gorgulla et al. “A multi-pronged approach targeting SARS-CoV-2 proteins using ultra-large virtual screening”. In: *iScience* 24.2 (2021), p. 102021. issn: 2589-0042. doi: <https://doi.org/10.1016/j.isci.2020.102021>. url: <https://www.sciencedirect.com/science/article/pii/S2589004220312189>.
- [24] Lorenzo Casalino et al. “AI-Driven Multiscale Simulations Illuminate Mechanisms of SARS-CoV-2 Spike Dynamics”. In: *bioRxiv* (2020). doi: 10.1101/2020.11.19.390187. eprint: <https://www.biorxiv.org/content/early/2020/11/20/2020.11.19.390187.full.pdf>. url: <https://www.biorxiv.org/content/early/2020/11/20/2020.11.19.390187>.
- [25] Kresten Lindorff-Larsen et al. “How Fast-Folding Proteins Fold”. In: *Science* 334.6055 (2011), pp. 517–520. issn: 0036-8075. doi: 10.1126/science.1208351. eprint: <https://science.sciencemag.org/content/334/6055/517.full.pdf>. url: <https://science.sciencemag.org/content/334/6055/517>.
- [26] Andre Merzky, Ole Weidner, and Shantenu Jha. “SAGA: A standardized access layer to heterogeneous distributed computing infrastructure”. In: *SoftwareX* 1 (2015), pp. 3–8.
- [27] Andre Merzky et al. “Design and Performance Characterization of RADICAL-Pilot on Leadership-class Platforms”. In: *arXiv preprint arXiv:2103.00091* (2021).
- [28] Andre Merzky et al. “Using pilot systems to execute many task workloads on supercomputers”. In: *Workshop on Job Scheduling Strategies for Parallel Processing*. Springer, 2018, pp. 61–82.
- [29] Vivek Balasubramanian et al. “Harnessing the power of many: Extensible toolkit for scalable ensemble applications”. In: *2018 IEEE International Parallel and Distributed Processing Symposium (IPDPS)*. IEEE, 2018, pp. 536–545.
- [30] Matteo Turilli, Mark Santcroos, and Shantenu Jha. “A comprehensive perspective on pilot-job systems”. In: *ACM Computing Surveys (CSUR)* 51.2 (2018), pp. 1–32.
- [31] Peter Eastman et al. “OpenMM 7: Rapid development of high performance algorithms for molecular dynamics”. In: *PLoS computational biology* 13.7 (2017), e1005659.
- [32] Kresten Lindorff-Larsen et al. “Improved side-chain torsion potentials for the Amber ff99SB protein force field”. In: *Proteins: Structure, Function, and Bioinformatics* 78.8 (2010), pp. 1950–1958.
- [33] Alexey Onufriev, Donald Bashford, and David A Case. “Exploring protein native states and large-scale conformational changes with a modified generalized born model”. In: *Proteins: Structure, Function, and Bioinformatics* 55.2 (2004), pp. 383–394.
- [34] James A Maier et al. “ff14SB: improving the accuracy of protein side chain and backbone parameters from ff99SB”. In: *Journal of chemical theory and computation* 11.8 (2015), pp. 3696–3713.
- [35] Hyungro Lee et al. “DeepDriveMD: Deep-Learning Driven Adaptive Molecular Simulations for Protein Folding”. In: *2019 IEEE/ACM Third Workshop on Deep Learning on Supercomputers (DLS)*. IEEE, 2019, pp. 12–19. doi: 10.1109/DLS49591.2019.00007. eprint: 1909.07817.
- [36] Junmei Wang et al. “Automatic atom type and bond type perception in molecular mechanical calculations”. In: *Journal of molecular graphics and modelling* 25.2 (2006), pp. 247–260.
- [37] Junmei Wang et al. “Development and testing of a general amber force field”. In: *Journal of computational chemistry* 25.9 (2004), pp. 1157–1174.
- [38] Tom Darden, Darrin York, and Lee Pedersen. “Particle mesh Ewald: An N·log(N) method for Ewald sums in large systems”. In: *The Journal of Chemical Physics* 98.12 (1993), pp. 10089–10092. doi: 10.1063/1.464397. eprint: <https://doi.org/10.1063/1.464397>. url: <https://doi.org/10.1063/1.464397>.
- [39] Debsindhu Bhowmik et al. “Deep clustering of protein folding simulations”. In: *BMC Bioinformatics* 19.18 (2018), p. 484.

- DOI: 10.1186/s12859-018-2507-5. URL: <https://doi.org/10.1186/s12859-018-2507-5>.
- [40] François Chollet. *Keras*. <https://github.com/fchollet/keras>. 2015.
- [41] Martín Abadi et al. *TensorFlow: Large-Scale Machine Learning on Heterogeneous Systems*. Software available from tensorflow.org. 2015. URL: <https://www.tensorflow.org/>.
- [42] Adam Paszke et al. “PyTorch: An Imperative Style, High-Performance Deep Learning Library”. In: *Advances in Neural Information Processing Systems 32*. Ed. by H. Wallach et al. Curran Associates, Inc., 2019, pp. 8024–8035. URL: <http://papers.nips.cc/paper/9015-pytorch-an-imperative-style-high-performance-deep-learning-library.pdf>.
- [43] Martin Ester et al. “A density-based algorithm for discovering clusters in large spatial databases with noise”. In: AAAI Press, 1996, pp. 226–231.
- [44] F. Pedregosa et al. “Scikit-learn: Machine Learning in Python”. In: *Journal of Machine Learning Research* 12 (2011), pp. 2825–2830.
- [45] Markus M Breunig et al. “LOF: identifying density-based local outliers”. In: *Proceedings of the 2000 ACM SIGMOD international conference on Management of data*. 2000, pp. 93–104.
- [46] T. Hricik, D. Bader, and O. Green. “Using RAPIDS AI to Accelerate Graph Data Science Workflows”. In: *2020 IEEE High Performance Extreme Computing Conference (HPEC)*. 2020, pp. 1–4. DOI: 10.1109/HPEC43674.2020.9286224.
- [47] Samuel Colvin. *Pydantic*. URL: <https://github.com/samuelcolvin/pydantic>. (accessed: 04.09.2021).
- [48] Mike Folk et al. “An overview of the HDF5 technology suite and its applications”. In: *Proceedings of the EDBT/ICDT 2011 Workshop on Array Databases*. 2011, pp. 36–47.
- [49] William F Godoy et al. “ADIOS 2: The Adaptable Input Output System. A framework for high-performance data management”. In: *SoftwareX* 12 (2020), p. 100561.
- [50] Eugen Hruska et al. “Extensible and Scalable Adaptive Sampling on Supercomputers”. In: *Journal of Chemical Theory and Computation (accepted)* (2020). <https://arxiv.org/abs/1907.06954>.
- [51] Yihang Wang, João Marcelo Lamim Ribeiro, and Pratyush Tiwary. “Past–future information bottleneck for sampling molecular reaction coordinate simultaneously with thermodynamics and kinetics”. In: *Nature Communications* 10.1 (2019), p. 3573. DOI: 10.1038/s41467-019-11405-4. URL: <https://doi.org/10.1038/s41467-019-11405-4>.